Harnessing negative refraction and evanescent waves toward super-resolution Lamb wave imaging

Hrishikesh Danawe[1] and Serife Tol[1]
Department of Mechanical Engineering, University of Michigan, Ann Arbor, MI USA 48109

(*Electronic mail: stol@umich.edu.)

(Dated: 5 July 2023)

We numerically and experimentally demonstrate super-resolution focusing of the lowest anti-symmetric (A0) mode Lamb waves in a thin aluminum plate. The subwavelength focusing/imaging is achieved by exploiting the anisotropy in phononic crystal (PC) lattices and amplification of evanescent waves. To this end, we embedded a PC flat lens in the aluminum plate, consisting of through holes arranged in a square lattice formation. We revealed that the bound slab phonon modes amplify evanescent waves, as previously observed for electromagnetic and acoustic waves. Hence, the slab mode helps propagate subwavelength information through the PC lens to reach the near-field image formed due to negative refraction and result in the high resolution image.

The imaging resolution of traditional imaging techniques is limited by the diffraction limit because of which conventional lenses cannot reproduce features smaller than half the wavelength (λ). The diffraction limit of 0.5λ arises due to the loss of the evanescent component of waves that carry subwavelength information from the source. The inherent spatial decay of evanescent waves prevents their contribution to image formation. In the late 1900s, Veslagos's (1968)[1] discovery of left-handed (LHMs) paved the path for the creation of flat optical lenses that can produce images via the unusual phenomenon of negative refraction not found within conventional materials. The negative refraction also enables the amplification of the evanescent component of the waves leading to super-resolution, which was first observed by Pendry (2000)[2] using an optical superlens. Apart from LHMs, artificially engineered periodic structures called photonic crystals were found to show negative refraction of electromagnetic waves due to negative group velocity in the second (or higher) phonon band leading to subwavelength imaging[3,4]. In the last two decades, subwavelength imaging using negative refraction has received considerable research attention not only for electromagnetic waves but also for acoustic and elastic waves due to their potential to benefit many applications, such as biomedical imaging, non-destructive testing, and ultrasonic imaging. Analogous to photonic crystals, phononic crystals (PCs) enable negative refraction and subwavelength imaging for acoustic or elastic waves due to the backward wave effect[5–10].

Although subwavelength focusing/imaging was observed using photonic and phononic crystals, breaking the diffraction limit requires a resonant coupling mechanism for amplifying large evanescent wavevectors. Super-resolution imaging was realized via the so-called canalization mechanism in the first phonon band of photonic/phononic crystals due to Fabry-Pérot resonance[11,12] and with resonant metamaterials such as superlenses[13–17], hyperlenses[18,19] and metalenses[19,20]. Luo et al. (2003)[21] attributed the resonant mechanism to be linked to the bounded modes of the photonic crystal slab in all angle negative refraction (AANR) regions in the second phonon band. Following their work, super-resolution was experimentally realized for acoustic waves by coupling evanescent waves with the bound slab mode of the PC slab[22]. Previously, super-resolution imaging has been demonstrated due to evanescent wave amplification via bound mode only for electromagnetic[21] and acoustic waves[22].

Besides electromagnetic and acoustic waves, subwavelength focusing and imaging of Lamb waves in thin elastic structures are of significant research interest due to their broad range of engineering applications. So far, different mechanisms utilizing PC flat lenses have been studied for subwavelength focusing/imaging of Lamb waves[9,10,23,24]. In our recent work[10], we demonstrated broadband subwavelength focusing of A0 mode Lamb wave by exploiting the anisotropy of a square lattice PC. We verified an image resolution of 0.63λ in the range between 60 kHz to 100 kHz. Dubois et al. (2015)[25] observed super-resolution imaging of flexural Lamb wave with a PC flat lens in the first phonon band, but it was attributed to time-driven super-oscillations rather than evanescent wave amplification. Further, metamaterial lenses composed of locally resonating unit cells were numerically demonstrated to show super-resolution imaging using surface flexural waves in thin plates[16,17]. In this Letter, we investigate the super-resolution focusing of flexural Lamb waves by coupling evanescent waves with the bound phonon slab mode of the square lattice PC slab. We experimentally verify imaging resolution better than 0.5λ using the PC flat lens.

We chose a simple square lattice design for the phononic crystal, which consists of through holes drilled into an aluminum plate. The unit cell of the PC is shown in the inset of Fig. 1 (a), with a side length of $a = 12.7$ mm and a hole diameter of 12 mm. The PC with four-unit cell rows in the longitudinal direction is embedded in the aluminum plate of thickness $t_p = 6.35$ mm with the ΓX crystal direction oriented along the interface of the plate and PC, as depicted in Fig. 1 (a). The thickness of the plate is reduced to half from $0.5a$ to $0.25a$ in the PC region. The focusing phenomenon via negative refraction in the PC lens is depicted using black and red arrows drawn from source to image that represent the wave vectors of propagating waves and the amplification direction of evanescent waves, respectively. In our previous work[9], a triangular lattice PC lens design with a step change in plate thickness was demonstrated for AANR in the second phonon band. Here, we have adopted the step change design with a square lattice PC to demonstrate super-resolution imaging via

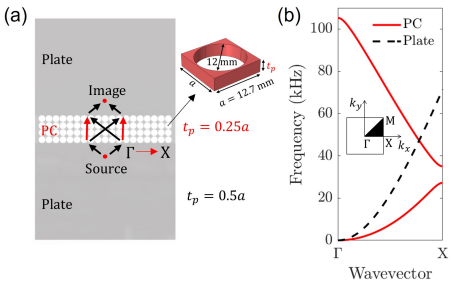

FIG. 1. (a) Flat PC lens embedded in an aluminum plate with a step change in plate thickness. The black and red arrows drawn from source to image represent the wave vectors of propagating waves and the amplification direction of evanescent waves, respectively. The unit cell of the PC is shown in the inset. (b) Dispersion band structure of the aluminum plate and PC with the plate thickness of $t_p = 0.5a$ and $t_p = 0.25a$, respectively, where a is the unit cell length. The first Brillouin zone of the square lattice is shown in the inset.

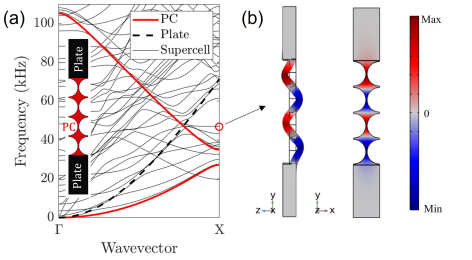

FIG. 2. (a) Dispersion band structure of supercell along with the band structure of the aluminum plate and PC. The supercell is depicted in the inset. (b) Modeshape of the supercell for the bound phonon slab mode with a flat dispersion band near 47 kHz.

negative refraction and evanescent wave amplification. The dispersion band structures of the aluminum plate and PC for plate thickness of $t_p = 0.5a$ and $t_p = 0.25a$, respectively, are shown in Fig. 1 (b) for the flexural (A0) Lamb mode. The first Brillouin zone of the square lattice is shown in the inset in wavevector or reciprocal space. The band structures are obtained using eigenfrequency analysis in COMSOL Multiphysics with Floquet periodicity boundary conditions at unit cell sides for the wavevectors lying in the first Brillouin zone of the PC. The material properties used for aluminum are: $\rho = 2700$ kg/m^3, $E = 70$ GPa, $\nu = .33$. The dispersion band of the plate intersects the second phonon band of the PC at about 47.2 kHz along the ΓX direction. On the other hand, the bands intersect at a higher frequency of 54.6 kHz along ΓM direction of the square lattice PC, which is oriented at 45° to ΓX direction because of the anisotropy. The anisotropy in square lattice arises due to the difference in the internal spacing between the neighboring holes along the two symmetry directions, ΓX and ΓM.

The super-resolution imaging is enabled by amplifying the evanescent waves by the bound slab phonon modes of the PC[21,22,26]. The bound slab modes are studied using a supercell of the flat lens, as shown in the inset of Fig. 2 (a). The supercell is a one-unit cell-wide slice cut out from the original lens along the longitudinal direction (see Fig. 1 (a)). Thus, the supercell consists of a four-unit cell-long PC segment squeezed in between the two plate segments on both sides. Periodic boundary conditions are applied at the supercell sides, and the band structure was obtained for transverse wave vectors along the interface of the lens (i.e., along ΓX direction). The band structure of the supercell is superimposed on top of the band structure of the PC and plate to identify the bound slab modes, as shown in Fig. 2 (a). The supercell bands lying below the plate band are called bound modes as they are bounded to the PC slab and travel along the transverse (ΓX) direction. The bound modes cannot propagate in the plate because the wavevector of these modes is greater than the maximum wavevector of propagating modes. The bound mode that couples with the evanescent waves of the plate have a nearly flat dispersion band in the AANR frequency range at 47 kHz. The band intersects the plate band at 48.2 kHz before converging at 47 kHz near the X point of the Brillouin zone. The mode shape of the supercell for the bound mode at 47 kHz is shown in Fig. 2 (b), depicting the deformation of the supercell bounded within the PC slab section. The photonic crystal studied by Luo et al. (2003)[21] has a similar flat band corresponding to a bound state in the AANR region of the second phonon band. They show that the bound photon state inside the slab leads to a resonance condition that amplifies the evanescent waves if the incident wave is sufficiently close to flat band frequency. Their flat band spans over a larger range of wavevectors due to the non-dispersive band of air for electromagnetic wave propagation. In contrast, the dispersion band of the flexural Lamb mode of the plate is parabolic in shape leading to a shorter flat band of the bound slab mode. The termination of the flat band at the boundary of the first Brillouin zone puts a limitation on the resolution of the image form due to AANR. The maximum possible evanescent wavevector that is amplified by the bound modes in the first Brillouin zone is π/a. However, the flat phonon band extends beyond the first Brillouin zone up to $(2\pi/a - k)$, where k is the wavevector in the plate at the operating frequency. Thus, the ultimate resolution limit estimated by Luo et al. (2003)[21] for their photonic crystal lens falls between $0.5a\lambda/(\lambda - a)$ and a. We chose the operating frequency of 49 kHz, which is close to the bound mode frequency, to demonstrate the super-resolution imaging. The wavevector in the plate at 49 kHz equals $k = 0.1962$ mm^{-1} ($\lambda = 32.04$ mm), which results in the ultimate imaging resolution staying between 0.33λ to 0.40λ.

To demonstrate super-resolution imaging, we constructed a phononic crystal flat lens using a 6.35 mm thick aluminum plate of side length 457.2 mm. The plate thickness was reduced to half in the PC slab region, and through holes were drilled through the reduced thickness. The array size of the holes was 4 x 35 with four rows in the longitudinal direction. The experimental setup is shown in Fig. 3. The alu-

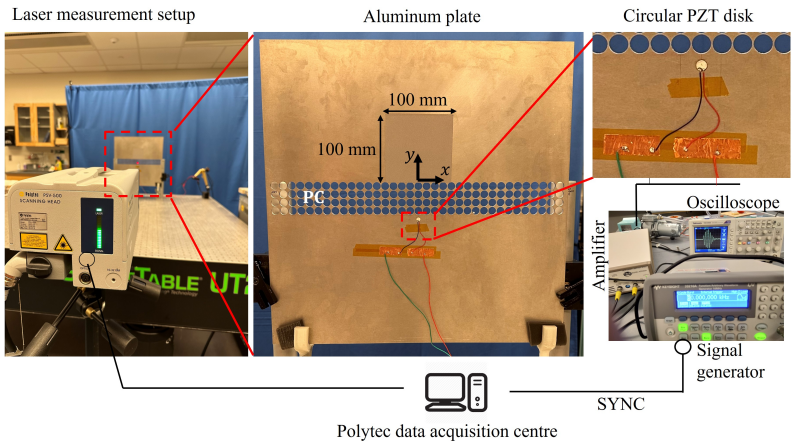

FIG. 3. Experimental setup for measuring the velocity field in the image region using a laser Doppler vibrometer. A piezoelectric (PZT) disk acts as an omnidirectional source of flexural Lamb waves. Two copper strips below the PZT disk are used to facilitate the electrical contact between the PZT leads and ends of the cable connected to the amplifier.

minum plate with the embedded PC lens was mounted on a vibration isolation table using two side supports. A PSV 500 scanning laser Doppler vibrometer was used to measure the velocity field on the plate surface in the image region of the lens. The spatial resolution of 0.1 mm (0.0031λ) is used for sampling the wavefield in the image region. A thickness mode piezoelectric (PZT) disk excites the flexural Lamb mode of the plate on one side of the PC slab, thus, behaving as a source. The diameter of the disk is 7mm ($< \lambda/4$) which is less than the quarter wavelength at the operating frequency. The PZT disk was vacuum bonded using epoxy near the bottom lens interface at a distance of $0.5a$ ($< \lambda/4$). Note that since the evanescent waves decay in space, the excitation source needs to be very close to the lens interface for efficient coupling of the evanescent waves with the bound slab mode. Hence, we chose to keep the source at a distance much less than the wavelength at the operating frequency. The PZT disk was excited with a twelve-cycle sine burst generated by a signal generator and amplified with a power amplifier. The measured data was stored in the Polytec data acquisition center while keeping the laser measurements in sync with the signal generator. The experiments were run at the operating frequency of 49 kHz for a sample time of 400μsec with a sampling frequency of 6.25 MHz. The experimentally measured full wavefield is provided in the supplemental material.

The normalized root mean square (RMS) velocity field measured by the laser in a 100 x 100 mm image region near the top lens interface is shown in Fig. 4 (a) after 300μsec. The image is formed right at the top lens interface with side lobes that are the characteristic feature of bound slab modes. The imaging phenomenon was also studied via time domain numerical simulation by replicating the experimental model in COMSOL Multiphysics with low-reflecting boundary conditions at the edges. The normalized RMS velocity field calculated using the numerical model is shown in Fig. 4 (b). The numerical velocity map is in good agreement with the experimental velocity map. We further obtained the line velocity plots along longitudinal and transverse directions passing through the highest intensity point of the image. The line plots are compared for the experiments and simulations, as shown in Fig. 4 (c)-(d). The line plots match very well except for the slightly higher amplitude of side lobes in experiments because of the boundary reflections at the plate edges and from the supports that hold the plate as no absorbing boundary conditions were applied in experiments. Nevertheless, the excellent match of the central peak in simulation and experiment shows that with a finite sine burst excitation signal the edge reflections do not affect the observed imaging resolution. We define the image resolution using full width at half maximum (FWHM) of the line velocity plot along the transverse direction. The FWHM is 14.5 mm (0.45λ) which overcomes the Rayleigh diffraction limit of 0.5λ. Thus, we conclude that the evanescent waves contribute to the reconstruction of the image. The evanescent wave amplification is linked to the overall resonance phenomenon of the bounded slab modes under the condition of transverse waveguiding via total internal reflection[21]. A finite and strong amplification of evanescent waves results when the incident wave does not exactly satisfy but is sufficiently close to this condition of overall resonance. We prove the existence of bounded phonon slab mode in our PC lens with the supercell study where the bounded mode modeshape is localized in between the two lens interfaces (see Fig. 2). We operate close to phonon band frequency and the side lobes along the transverse direction (i.e., along the interface of the lens) which decay in amplitude away from the central peak (see Fig. 4(c)) further confirm the role of bounded

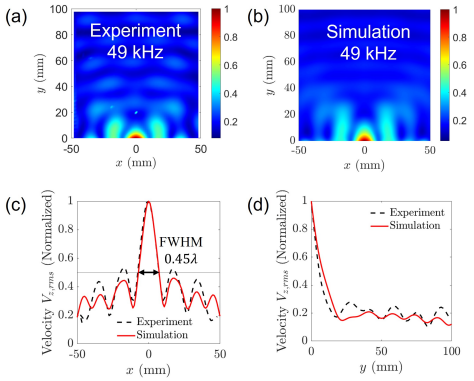

FIG. 4. (a) Normalized root mean square (RMS) velocity field measured in experiments. (b) Normalized RMS velocity field calculated via simulations. (c) Line velocity plot along x-direction passing through the highest intensity point in the image. (d) Line velocity plot along y-direction passing through the highest intensity point in the image.

phonon slab modes in the amplification of evanescent waves contributing to the image formation. Note that the imaging resolution is a function of time as previously observed for an acoustic lens by Robillard et al. (2015)[26]. The resolution gets better with time and reaches close to the ultimate resolution limit in the range $[0.33\lambda, 0.40\lambda]$ if sufficient time is allowed for a steady-state image formation. In our experimental setup, there is a limitation on the number of cycles that we excite due to the finite length of the plate, thus the imaging resolution could only reach 0.45λ. As time passes, the reflected waves from boundaries start to interfere strongly in the image region, thus, prohibiting the steady state image formation. Nonetheless, we have demonstrated super-resolution focusing using flexural lamb waves in a phononic crystal flat lens via the amplification of evanescent waves by the bound slab mode.

In summary, this Letter presents an approach for super-resolution imaging of flexural Lamb waves in a thin aluminum plate using a flat PC lens. The lens has a step-change of plate thickness to achieve AANR in the second phonon band of the PC. We found the existence of a bound slab phonon mode in the AANR region with a flat dispersion band similar to the photonic crystal of Luo et al. (2003). The bound slab mode couples with the evanescent waves coming from the source and enable them to propagate the subwavelength information to the image plane. A near-field super-resolution image formation is experimentally and numerically demonstrated using the proposed lens design with an excellent agreement between measured and calculated velocity fields in the experiments and simulations, respectively. The resolution of 0.45λ is achieved in the current experimental setup which is less than the diffraction limit of 0.5λ. We exploited the bound slab modes for evanescent wave amplification resulting in super-resolution imaging of A0 mode Lamb waves. The characteristic feature of bound slab modes is observed in the image, indicating their role in the contribution of evanescent waves to the image formation. This study may benefit the future implementation of superlenses for focusing of flexural waves in thin elastic structures pertaining to applications such as structural health monitoring, non-destructive testing, and energy harvesting.

See the supplementary material for the full wavefield measured in the experiments.

This work was supported by the National Science Foundation under Grant No. CMMI-1914583.

AUTHOR DECLARATIONS

Conflict of Interest

The authors have no conflicts to disclose.

DATA AVAILABILITY

The data that support the findings of this study are available from the corresponding author upon reasonable request.

[1]V. G. Veselago, "The electrodynamics of substances with simultaneously negative values of ε and μ," Sov. Phys. Uspekhi **10**, 509–514 (1968).
[2]J. B. Pendry, "Negative refraction makes a perfect lens," Phys. Rev. Lett. **85**, 3966–3969 (2000).
[3]A. Berrier, M. Mulot, M. Swillo, M. Qiu, L. Thylén, A. Talneau, and S. Anand, "Negative refraction at infrared wavelengths in a two-dimensional photonic crystal," Phys. Rev. Lett. **93**, 073902 (2004).
[4]R. Moussa, S. Foteinopoulou, L. Zhang, G. Tuttle, K. Guven, E. Ozbay, and C. M. Soukoulis, "Negative refraction and superlens behavior in a two-dimensional photonic crystal," Phys. Rev. B **71**, 085106 (2005).
[5]M. Ke, Z. Liu, C. Qiu, W. Wang, J. Shi, W. Wen, and P. Sheng, "Negative-refraction imaging with two-dimensional phononic crystals," Phys. Rev. B **72**, 064306 (2005).
[6]C. Qiu, X. Zhang, and Z. Liu, "Far-field imaging of acoustic waves by a two-dimensional sonic crystal," Phys. Rev. B **71**, 054302 (2005).
[7]A. Sukhovich, L. Jing, and J. H. Page, "Negative refraction and focusing of ultrasound in two-dimensional phononic crystals," Phys. Rev. B **77**, 014301 (2008).
[8]C. Croënne, E. D. Manga, B. Morvan, A. Tinel, B. Dubus, J. Vasseur, and A.-C. Hladky-Hennion, "Negative refraction of longitudinal waves in a two-dimensional solid-solid phononic crystal," Phys. Rev. B **83**, 054301 (2011).
[9]H. Danawe and S. Tol, "Experimental realization of negative refraction and subwavelength imaging for flexural waves in phononic crystal plates," Journal of Sound and Vibration **518**, 116552 (2022).
[10]H. Danawe and S. Tol, "Broadband subwavelength imaging of flexural elastic waves in flat phononic crystal lenses," Scientific Reports **13**, 7310 (2023).
[11]P. A. Belov, C. R. Simovski, and P. Ikonen, "Canalization of subwavelength images by electromagnetic crystals," Phys. Rev. B **71**, 193105 (2005).
[12]Z. He, F. Cai, Y. Ding, and Z. Liu, "Subwavelength imaging of acoustic waves by a canalization mechanism in a two-dimensional phononic crystal," Applied Physics Letters **93**, 233503 (2008).
[13]S. Zhang, L. Yin, and N. Fang, "Focusing ultrasound with an acoustic metamaterial network," Phys. Rev. Lett. **102**, 194301 (2009).
[14]J. J. Park, C. M. Park, K. J. B. Lee, and S. H. Lee, "Acoustic superlens using membrane-based metamaterials," Applied Physics Letters **106**, 051901 (2015).
[15]M. Chen, H. Jiang, H. Zhang, D. Li, and Y. Wang, "Design of an acoustic superlens using single-phase metamaterials with a star-shaped lattice structure," Scientific Reports **8** (2018).
[16]M. Farhat, S. Enoch, and S. Guenneau, "Biharmonic split ring resonator metamaterial: Artificially dispersive effective density in thin periodically perforated plates," Europhysics Letters **107**, 44002 (2014).
[17]Z. Wang and T. Li, "Superlensing effect for flexural waves on phononic thin plates composed by spring-mass resonators," AIP Advances **9** (2019), 085207.

[18]J. Li, L. Fok, X. Yin, G. Bartal, and X. Zhang, "Experimental demonstration of an acoustic magnifying hyperlens," Nature materials **8**, 931–4 (2009).
[19]D. Lu and Z. Liu, "Hyperlenses and metalenses for far-field superresolution imaging," Nature communications **3**, 1205 (2012).
[20]J. Zhu, J. Christensen, J. Jung, L. Martin-Moreno, X. Yin, L. Fok, X. Zhang, and F. Garcia-Vidal, "A holey-structured metamaterial for acoustic deep-subwavelength imaging," Nature Physics **7**, 52–55 (2011).
[21]C. Luo, S. G. Johnson, J. D. Joannopoulos, and J. B. Pendry, "Subwavelength imaging in photonic crystals," Phys. Rev. B **68**, 045115 (2003).
[22]A. Sukhovich, B. Merheb, K. Muralidharan, J. O. Vasseur, Y. Pennec, P. A. Deymier, and J. H. Page, "Experimental and theoretical evidence for subwavelength imaging in phononic crystals," Phys. Rev. Lett. **102**, 154301 (2009).
[23]M. Farhat, S. Guenneau, S. Enoch, A. B. Movchan, and G. G. Petursson, "Focussing bending waves via negative refraction in perforated thin plates," Applied Physics Letters **96** (2010).
[24]M. Dubois, M. Farhat, E. Bossy, S. Enoch, S. Guenneau, and P. Sebbah, "Flat lens for pulse focusing of elastic waves in thin plates," Appl. Phys. Lett. **103**, 071915 (2013).
[25]M. Dubois, E. Bossy, S. Enoch, S. Guenneau, G. Lerosey, and P. Sebbah, "Time-driven superoscillations with negative refraction," Phys. Rev. Lett. **114**, 013902 (2015).
[26]J.-F. Robillard, J. Bucay, P. A. Deymier, A. Shelke, K. Muralidharan, B. Merheb, J. O. Vasseur, A. Sukhovich, and J. H. Page, "Resolution limit of a phononic crystal superlens," Phys. Rev. B **83**, 224301 (2011).